Preprint Title	Investigation of memory effect in Au/(Ti-Cu)Ox-gradient thin film/ TiAlV structure
Authors	Damian Wojcieszak, Jarosław Domaradzki, Michał Mazur, Tomasz Kotwica and Danuta Kaczmarek
Publication Date	05 Oct 2021
Article Type	Full Research Paper
ORCID® iDs	Damian Wojcieszak - https://orcid.org/0000-0001-6831-4477; Michał Mazur - https://orcid.org/0000-0002-6997-4204

Title Investigation of memory effect in Au/(Ti-Cu)Ox-gradient thin film/TiAlV structure

*Damian Wojcieszak *, Jarosław Domaradzki, Michał Mazur, Tomasz Kotwica, Danuta Kaczmarek*

Wrocław University of Science and Technology, Faculty of Electronics, Photonics and Microsystems, Janiszewskiego 11/17, 50-372 Wroclaw, Poland

E-mail: damian.wojcieszak@pwr.edu.pl

Keywords: resistive switching, memory effect, gradient thin film, magnetron sputtering

Abstract: The paper presents the results of the analysis of resistive switching properties observed in (Ti-Cu)-oxide thin film with gradient distribution of elements over the thin film thickness. Thin films were prepared using the multisource reactive magnetron co-sputtering process. Programmed profile of the pulse width modulation coefficient during sputtering of the Cu target allowed to obtain the designed gradient U-shape profile of Cu concentration in the deposited thin film. Electrical measurements of Au/(Ti-Cu)Ox/TiAlV structure showed the presence of nonpinched hysteresis loops in the voltage–current plane testifying the resistive switching behavior. Additionally, the initial forming process of conducting filaments has been observed as well. Optical, x-ray, and ultraviolet photoelectron spectroscopy measurements allowed to create the scheme of the bandgap alignment of the prepared thin films with respect to the Au and TiAlV electrical contacts. Detailed structure and elemental profile investigations allowed to conclude about the presence of conducting filaments of the observed resistive switching mechanism occurring in the prepared test structure. The obtained results showed that the prepared gradient (Ti-Cu)Ox thin film could be an interesting alternative to the conventional multilayer stack construction of resistive switching devices.

1. Introduction

In recent years, a significant development in designing, simulation, manufacturing, and characterization methods has been observed for devices with the ability to switch between two resistance states: the low (LRS) and the high resistance state (HRS) namely the resistive switching devices. This increase is due to a possible application area of such devices in the fields of neuromorphic [1-4] and chaotic systems [5,6], textile electronics [7], and even quantum systems. [8] The resistive switching devices have already found their place in the field of memory applications, especially in nonvolatile memory such as resistive random-access memory (RRAM) [9-13] or conducting bridge random-access memory (CBRAM). [14] Resistive switching devices are usually made in the form of a metal-insulator-metal (MIM) structure. [e.g. 15] Commonly, such structures are fabricated in the form of a stack of multilayers consisting of a very thin (several-dozen nanometers) isolated oxide layer and a much wider (several hundred nanometers) doped (or nonstoichiometric) layer. Materials used for such multilayers vary from HfO_2 (e.g. [3,16-19]), ZnO (e.g. [20,21]), CuO (e.g. [22-28]), ZrO_2 [29] Ta_2O_5 (e.g. [30,31]) or NiO [32-35]. However, the most commonly used material as the active layer in resistive switching devices is TiO_{2-x} (e.g., [36-41]). In addition, a crucial role in the resistive switching mechanism plays the material used for metal electrodes. Usually such materials are used as Au, Ag, Ni, Ti, W, TiN, or ITO [2,22,42]. Some examples of resistive switching behavior were also found in structures based on nanowires [43] or nanotubes [26,43], where the resistive switching device is characterized by the presence of a pinched or nonpinched hysteresis loop in the I-V characteristics in the DC plane.

In the present paper, the results of the analysis carried out for (Ti-Cu)-oxide semiconducting thin film placed between Au and Ti6Al4V metal electrodes have been presented. Contrary to the results presented in the literature, experimental electrical measurements performed for DC simulation showed bipolar resistive switching properties which were observed not for a conventional multilayer stack construction but for a single thin

film with the gradient distribution of the elements over the thickness of the structure. The (Ti-Cu)-oxide semiconducting thin film with U-shape like distribution profile of copper allowed to observe nonpinched hysteresis loops with the addition of the forming curve. The fabricated structures showed a hysteresis (memory) loop under both positive and negative bias conditions, and the conducting filament type of switching was indicated based on the performed investigations. The discussions on the possible explanation of the observed electrical behavior in the prepared structures were supported with investigations of surface properties performed using X-ray and UV photoelectron spectroscopy, and cross-sectional elemental analysis.

2. Experimental

The deposition system and the method for the preparation of gradient thin films with different profiles of element concentration have already been described in detail in [44-48]. The thin films were deposited in a reactive mode in the magnetron co-sputtering process, using two circular titanium targets (99.995%) and one circular copper target (99.995%). Targets were sputtered simultaneously in an oxygen atmosphere of 99.999% purity. The targets used in the process were 28.5 mm in diameter and their thickness was 3 mm [50]. The process uses magnetrons with an unbalanced magnetic field set in a confocal configuration vs. the substrate. The target-substrate distance was 14 cm. Before the deposition process, the working chamber was pumped down to a pressure of 10^{-3} Pa. Thin films were sputtered without additional intentional heating of the substrates during the process. Each magnetron was powered with a separate MSS2 power supply from Dora Power System [49]. The applied power supply allowed to obtain a maximum power of up to 2 kW in the unipolar pulsed DC mode. The power delivered to the magnetrons was controlled independently for each of the magnetrons [47]. DC pulses of the magnetron power supply consisted of groups of unipolar sinusoidal pulses with a frequency of 140 kHz, while the power supplied to the magnetrons was regulated by changing the width of the groups of these pulses (PWM method - pulse width modulation). To obtain a gradient

distribution of elements as a function of the thickness of the deposited layers, magnetrons equipped with titanium targets were supplied with a constant coefficient pwm_{Ti} = 100% during the entire deposition process. On the contrary, the magnetron with the cooper target was powered by pulses with the pwm_{Cu} coefficient which value was changed from 60% to 10% and to 0% for the half of the time of deposition and then for the remaining half of the time of deposition, it was changed from 0% to 10% and to 60% (**Figure 8** – the U-shape like of powering profile). The total time of deposition was 240 minutes. The determined values of the pwm_{Ti} and pwm_{Cu} coefficients were selected on the basis of the performed series of preliminary deposition processes.

Due to the requirements of various measurement methods used to characterize the properties of the fabricated structures, thin gradient layers were deposited on silicon (Si), amorphous silica (SiO_2), and conductive metallic substrates (Ti6Al4V). The resulting thickness of the prepared thin film was about 610 nm as measured using a Talysurf optical profiler (Tylor Hobson CCI Lite). Additionally, circular 1 mm gold pads were evaporated at the top of the prepared structure to allow the electrical characterization. The average material composition of the gradient thin film was determined using x-ray microanalysis employing EDAX Genesis energy dispersive spectrometer (EDS) as a part of FESEM FEI Nova NanoSEM 230 scanning electron microscope. The content of Ti and Cu in the whole volume of the thin film was estimated to be 48 at% and 52 at%, respectively. Additionally, the material composition was determined without taking oxygen into consideration and no unintentional impurities were observed in the coating. Structural properties were analyzed using x-ray diffraction (XRD) and transmission electron microscopy (TEM). XRD patterns were obtained with the use of PANalytical Empyrean PIXed3D powder diffractometer with Cu Kα X-ray (1.5406 Å) and no diffraction peaks were observed testifying about the dominating amorphous nature of the deposited thin film. Microstructure of the (Ti-Cu)Ox film was further analyzed with the aid of a TECNAI G2 FEG Super-Twin (200 kV) transmission electron microscope equipped with

EDS attachment. The local chemical composition of the cross-section was also investigated to show the gradient distribution of Ti and Cu elements in function of the thin film depth. X-ray photoelectron spectroscopy (XPS) studies were performed to determine the chemical state of titanium and copper at the surface of mixed oxide thin films. The Specs XR-50 X-ray nonmonochromatic excitation source with Mg Kα (1253.6 eV) beam was used. The Specs Phoibos 100 MCD-5 (5 single channel electron multiplier) hemispherical analyzer was used to collect photoelectrons with a step size of 0.1 eV. All spectra were calibrated with respect to the binding energy of the adventitious C1s peak at 284.8 eV. Ultraviolet photoelectron spectroscopy (UPS) was performed using a nonmonochromatic He I line (21.22 eV) excitation source and a step size was equal to 0.025 eV. A bias voltage of -5 V was applied to the thin film sample during UPS measurement to obtain a clear secondary electron cut-off. Binding energies of the spectra were referred to the Fermi level (E_F) that was determined from the cleaned reference Au sample. Measurement results were analyzed with the aid of CasaXPS software. For the determination of the type of electrical conductivity, measurements of thermoelectrical Seebeck effect were conducted using the setup consisting of INSTEC chamber equipped with four electrical probes and two hot chucks, INSTEC MK1000 temperature controller and INSTEC LN2-P pump. The optical transmission coefficient in the visible part of the optical radiation was measured using QE6500 CCD scientific grade spectrophotometer (Ocean Optics). For the DC current-to-voltage electrical measurements, a Keithley SCS4200 semiconductor characterization system and a M100 Cascade Microtech probe station were used. All electrical measurements were performed in a controlled room temperature (23 °C) and humidity (30% RH) in ambient air.

3. Results

3.1. Electrical properties

Resistivity of as-deposited thin film was determined to be equal $1 \cdot 10^3$ Ωcm. The type of electrical conductivity was determined by the Seebeck coefficient measurements performed in the range from 25 °C to 125 °C. The result of the thermoelectric voltage as a function of the difference of temperature measured between two opposite electrical contacts is shown in **Figure 1**.

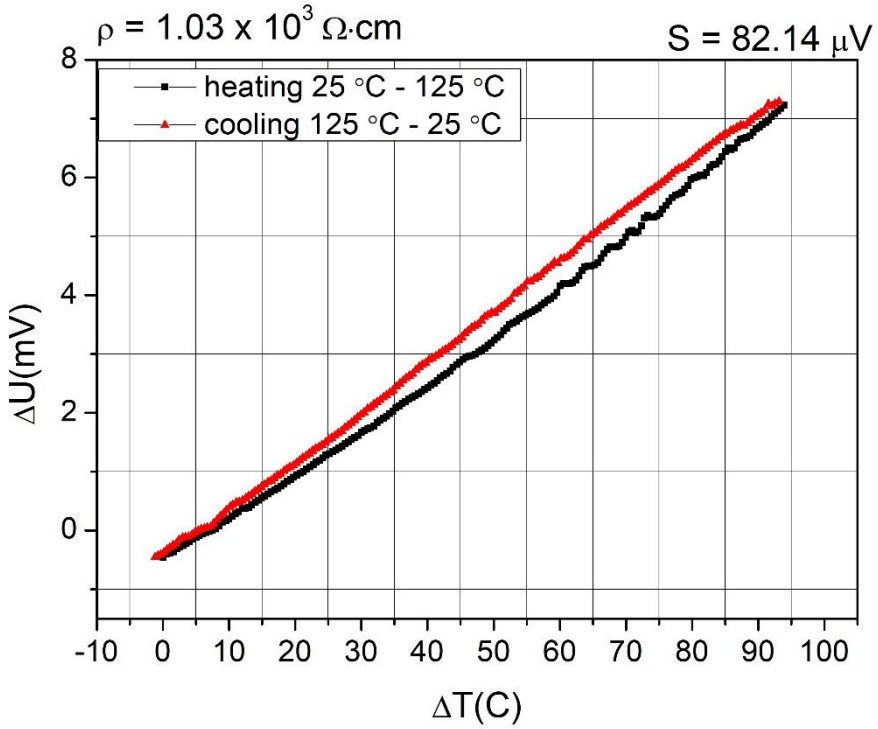

Figure 1. Thermovoltage characteristics measured for Au/(Ti-Cu)Ox/TiAlV thin film structure

The Seebeck coefficient (+82.14 μV) testified about p-type conductivity of the prepared gradient thin film. The p-type of electrical conduction is often reported for Cu_2O (or CuO) – based thin films, whereas TiO_2 is naturally n-type semiconducting oxide. [50, 51] In the presented case of the prepared mixed (Ti-Cu)Ox thin film, the obtained result testifies that holes were the majority charge carriers.

The DC measurements of the current-to-voltage characteristic were conducted in a transverse Au/(Ti-Cu)Ox/Ti6Al4V configuration system (**Figure 2**). The structure was powered by forcing the constant current which was swept from (0 nA) to (60 nA), then (60 nA) – (0 nA) – (-60 nA) and again from (-60 nA) – (0 nA) – (60 nA). Depending on the direction of the applied current, the structure was either in high (HRS) or in low (LRS) resistance state at the same value of the forcing current. When the direction of the current was changed to the opposite polarity, the structure still "remembered" its high resistance state until, again, the direction of the current was changed and the structure returned to its low resistance state. Measurements of I-V characteristics were performed in several tens of cycles.

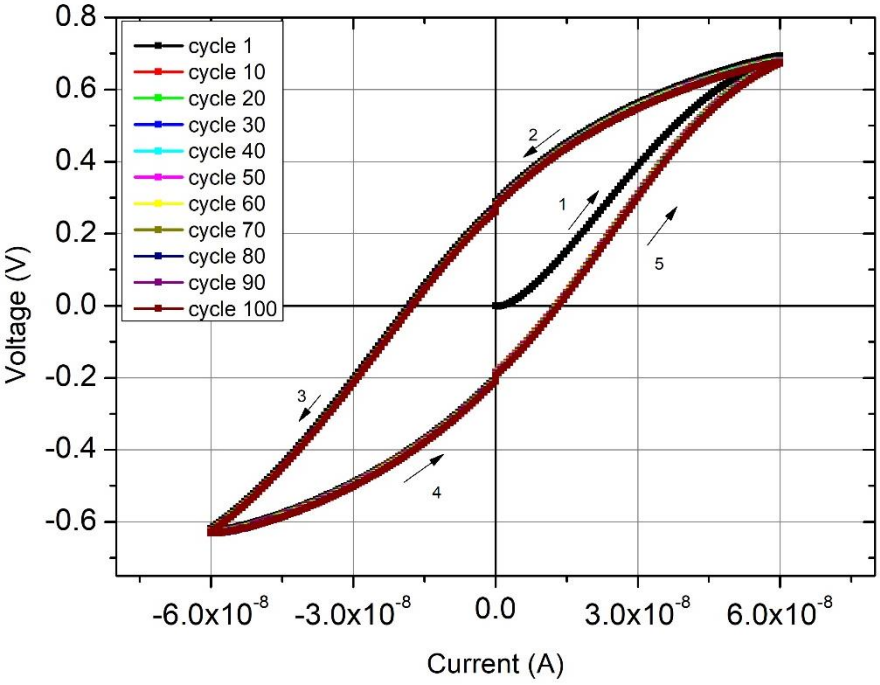

Figure 2. Direct current–voltage characteristics for Au/(Ti-Cu)Ox/TiAlV thin film structure. Arrows indicate the sequence of changing the current forcing during the measurements

Operation in Low Resistance State was reached when the forcing current was about $1.32 \cdot 10^{-8}$ A (or $-1.74 \cdot 10^{-8}$ A) that results in structure resistance of about 50 kΩ. However, for the same value of forcing current in High Resistance State, the structure resistance reached about 30 MΩ. Resistance-to-forcing current characteristics with observed switching behavior

are presented in **Figure 3**. Obtained results for the measured 100 cycles testify very good reproducibility and good stability (retention) of the prepared material – **Figure 4**. The difference in structure resistance in HR and LR states was about $6 \cdot 10^2$ times.

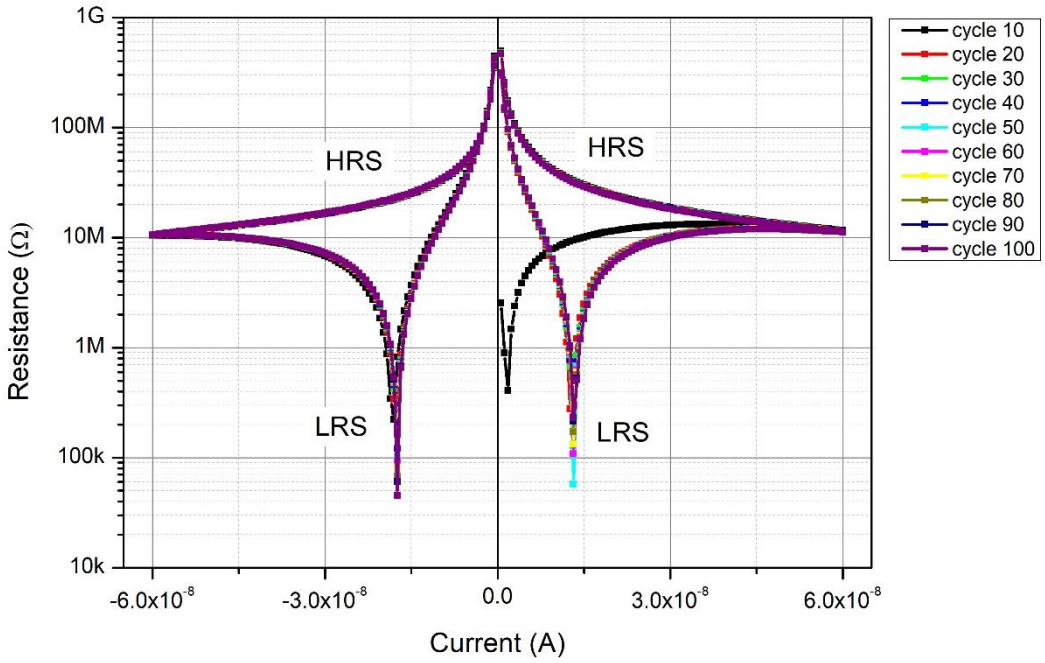

Figure 3. Switching characteristics for Au/(Ti-Cu)Ox/Ti6Al4V thin film structure as a function of forcing current for both directions of the current flow

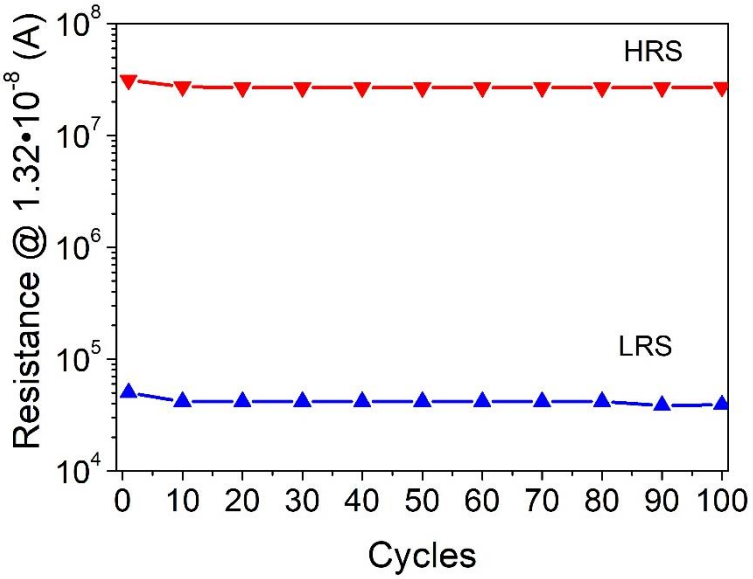

Figure 4. Retention characteristics for Au/(Ti-Cu)Ox/TiAlV thin film structure.

3.2. Optical properties

Figure 5 presents the transmission and reflection spectra for the prepared thin (Ti-Cu)Ox film. As one can see, the prepared thin film was relatively well transparent in the visible part of the optical radiation. However, the average transmission does not exceed more than 25 % on average in the wavelength range from 500 nm to 1000 nm. In the infrared, the transparency of the thin film is higher and reaches even 40 % on average. Visible maxima and minima result from multiple interferences of the light reflected from air-thin film and thin film-SiO_2 substrate. Recorded optical spectra allowed determining the optical bandgap width of about 2.8 eV for the allowed indirect transitions using the Tauc method.

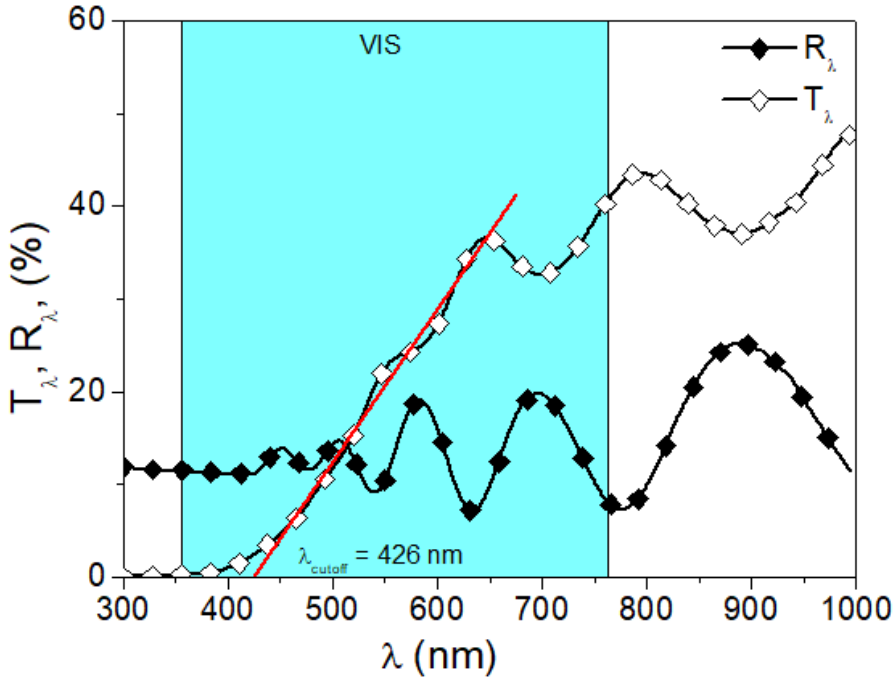

Figure 5. Results of transmission and reflection measurements for gradient (Ti-Cu)Ox thin film

3.3. Structure and elemental composition

3.3.1. Surface properties

The oxidation state of the copper at the surface of $(Ti_{0.48}Cu_{0.52})Ox$ thin film was analyzed with the use of XPS Cu2p core level as shown in **Figure 6**. The Cu2p core level has split spin-orbit components with ΔBE of 19.8 eV and the intensity ratio of $Cu2p_{1/2}$ and $Cu2p_{3/2}$ of ca. 0.5. The well-known fact is that it is possible to distinguish Cu oxidation states taking into consideration not only the position of $Cu2p_{3/2}$ peak but also the satellite features that could be visible above the binding energy of this peak. According to Biesinger [52,53], the shake-up satellite peaks are present for samples containing Cu^{2+} species but are absent for samples containing only Cu^0 and Cu^+ species. Therefore, in the case of the measured thin film, the binding energy of $Cu2p_{3/2}$ and the occurrence of the well-visible satellite peak at ca 940-945 eV indicates the presence of Cu^{2+} species related to the CuO oxide. [52-54]

The XPS spectrum of the Ti2p core level is presented in **Figure 6b**. The position of Ti2p doublet and the binding energy separation between $Ti2p_{3/2}$ and $Ti2p_{1/2}$ (marked in the figure as ΔE_W) equal to 5.8 eV testifies the +4 oxidation state of titanium present at the surface. The ratio of the area of the $Ti2p_{3/2}$ and $Ti2p_{1/2}$ peaks is equal to 2:1, confirming the presence of the stoichiometric TiO_2 at the surface of the mixed oxide $(Ti_{0.48}Cu_{0.52})Ox$ thin film. Furthermore, the O1s spectrum (**Figure 6c**) was deconvoluted into three peaks related to the lattice oxygen (for TiO_2 and CuO), hydroxyl radicals (OH^-) and adsorbed water molecules (H_2O_{ads}).

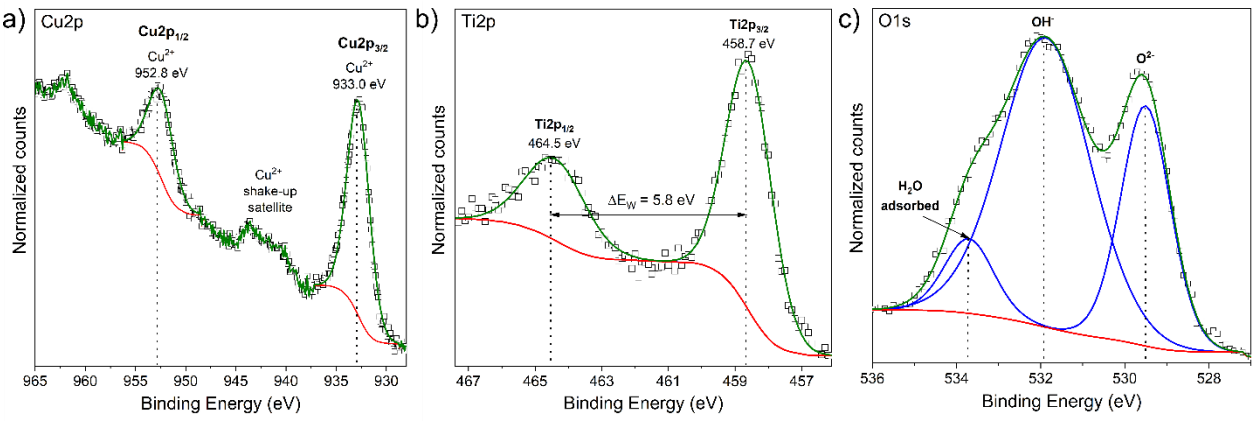

Figure 6. XPS spectra of the surface of $(Ti_{0.48}Cu_{0.52})Ox$ thin film: a) Cu2p, b) Ti2p, and c) O1s core levels

The UPS spectrum for the $(Ti_{0.48}Cu_{0.52})Ox$ thin film is shown in **Figure 7**. The position of the valence band maximum (VBM) was determined from the extrapolation of the line fit to the leading edge of the spectrum as marked in the **Figure 7a** and is at 1.20 eV below the Fermi level (E_F). Taking into consideration the band gap energy of the thin films equal to 2.80 eV, the thin film surface exhibits p-type conduction. The electron affinity (χ) of the thin film surface was equal to 2.41 eV and was calculated based on the relationship [55,56]:

$$\chi = h\nu - W - E_g \quad (1)$$

where: hν = 21.22 eV is the photon energy of He(I), W=16.01 eV is the spectrum width, i.e., the energy difference between the VBM and the cut-off energy of the photoemission, E_g=2.80 eV is the band gap energy calculated from the transmission spectrum.

The work function (W_f) was determined to be equal to 4.01 eV and was calculated as the difference between the photon energy of He(I) line and the position of the cut-off energy of the photoemission (17.21 eV).

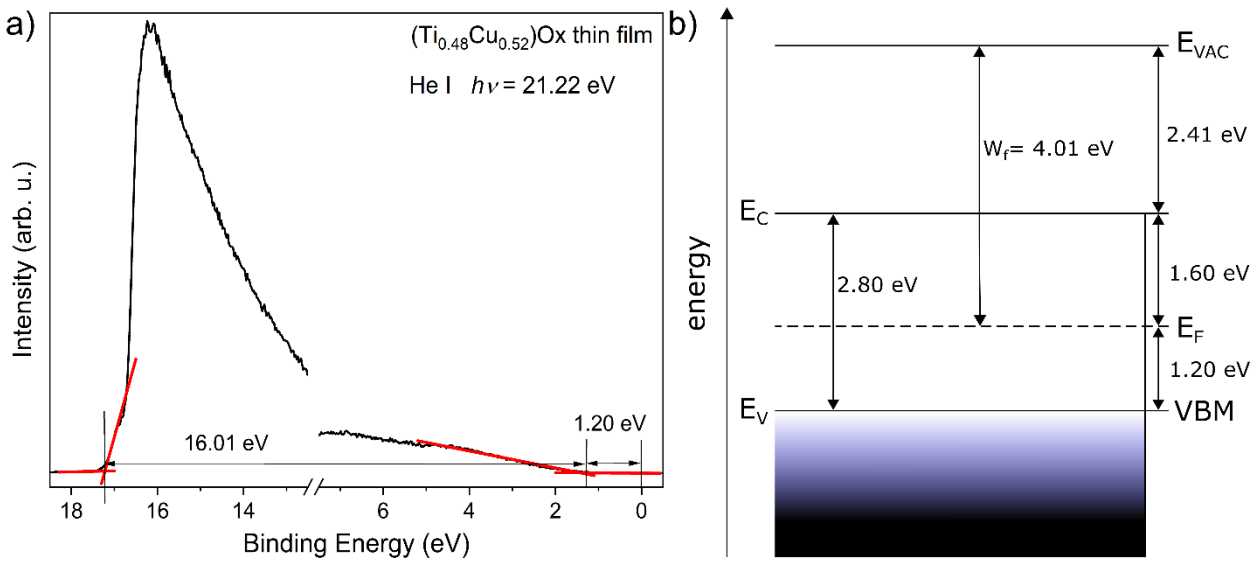

Figure 7. Photoelectron spectrum of a valence band (a) and schematic energy diagram (b) of the surface of $(Ti_{0.48}Cu_{0.52})Ox$ thin film

3.3.2. Cross section analysis

The structural investigations included measurements of the material composition using a scanning electron microscope (FEI-inspected S50) with an electron dispersion spectrometer (EDS) and the cross-sectional analysis of the prepared thin-film structures using a transmission electron microscope (TEM) with X-ray probe. With respect to the programmed U-shape of the magnetron powering profile, the distribution of elements versus the thickness of the deposited (Ti-Cu)Ox thin films consist of four parts. The first two parts include the decrease of copper in a more rapid way at the beginning of thin film deposition to ca. 80 nm and a moderate way for the next ca. 200 nm of the thin film thickness. After that, the content of copper in the thin film structure began to increase. The third part of the structure includes the point at ca. 350 nm, where the content of copper is the lowest, whereas the content of titanium is the highest. After that point, the content of copper started to increase for the next ca. 200 nm. The last, the fourth part, is the rapid increase in the content of copper for the next ca. 80 nm. The TEM and EDS (**Figure 8**) confirmed that the symmetrical U-shape-like gradient (Ti-Cu)Ox of the thin film was achieved. In addition, the structure of the prepared thin film could be also divided into three areas: 1) polycrystalline area located from the surface to the near-center of the structure, 2) amorphous area located from the center to the near-substrate region and 3) void rich area located from the near-substrate to the substrate region. In the middle of the structure there is clearly seen a very thin (c.a. 10 nm) region with different structural properties and chemical composition. As it results from the performed TEM analysis (**Figure 8**), it can be interpreted as a very dense amorphous area. What is more, during the deposition process, the flow of oxygen supplied to the working chamber was constant. Decreasing the power supplied to the magnetron with the copper target to 0% pwm results that all oxygen in the chamber was

consumed by the sputtered titanium targets. That resulted in the deposition of dense, amorphous TiO_2 just in the middle of the gradient thin film.

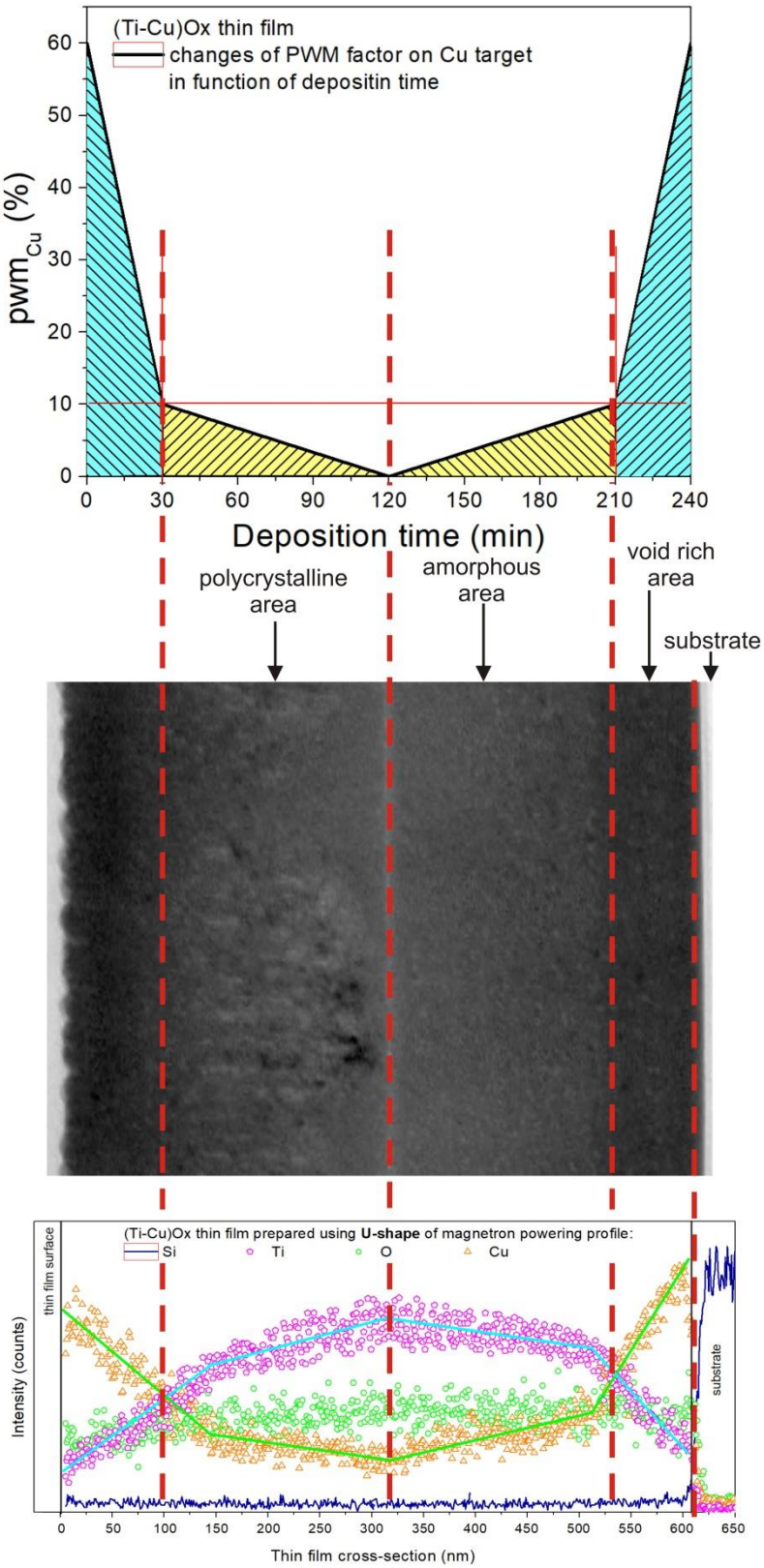

Figure 8. Results of TEM analysis and distribution of Cu,Ti,O,Si elements in gradient (Ti-Cu)Ox thin film with correlation to the U-shape like changes of the pwm coefficient

4. Discussion

According to the construction, structure and elemental analyses, four different boundaries can be recognized in the prepared thin film structure, i.e: Au – (Ti-Cu)Ox, (Ti-Cu)Ox – TiO_2, TiO_2 – (Ti-Cu)Ox and (Ti-Cu)Ox – Ti6Al4V. To further analyze the switching mechanism of the observed memory effect, the energy diagram was proposed in **Figure 9**. The constructed diagram assumes the presence of an additional wide TiO_2 region in the middle of the prepared structure that corresponds to the region of high Ti concentration in the central part of the prepared (Ti-Cu)Ox thin film. The value of the work function (5.4 eV) and the width of the optical energy gap (3.34 eV) for the TiO_2 were determined for a reference thin (about 100 nm thick) amorphous TiO_2 layer, prepared in the magnetron sputtering process using the same deposition system with the coefficient pwm_{Ti}=100 % during the entire sputtering process. The conducted analyzes allowed to conclude that both interfaces created at the border of either Au or Ti6Al4V and the deposited (Ti-Cu)Ox thin film were electrical ohmic contacts, because the value of the work function of Au (ΦAu = 5.3 eV) or (ΦTi6Al4V = 4.3 eV) is greater than the work function value of the (Ti-Cu)Ox layer (Φ(Ti-Cu)Ox = 4.01 eV). This conclusion is supported by the symmetrical shape of I-V curves measured in both directions of the forcing current (**Figure 2**). The measured nonpinched hysteresis shape of the I-V curves could be due to a wide (about 420 nm) area of the region rich in titanium oxide that results in a relatively high series resistance. We believe that in the discussed case, switching from a high to low resistance state connected with the formation of filament-type conduction paths allows electrical charge carriers to flow between two opposite contacts. Observed first cycle in I-V plane that differs from the rest of the results suggests the presence of the formation process of

the conducting paths, when for the first time the forcing current was applied to the investigated structure.

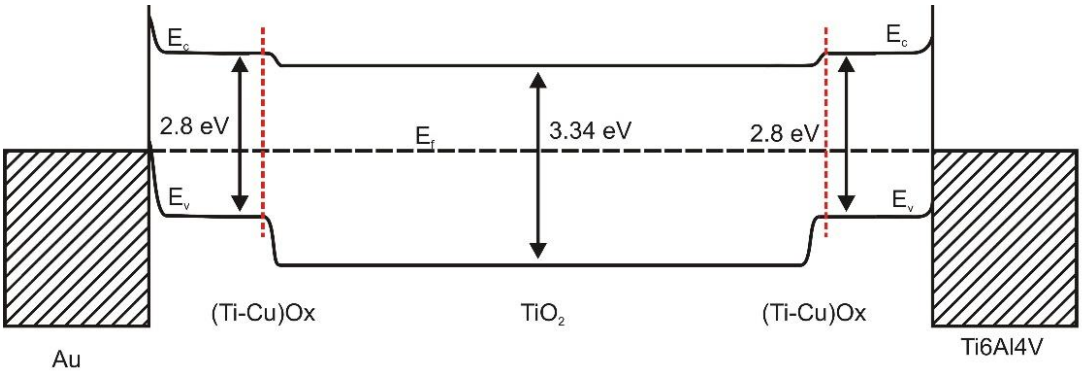

Figure 9. Schematic illustration of energy-level diagrams of the prepared Au/(Ti-Cu)Ox/Ti6Al4V structure

5. Conclusions

The paper presents the results of investigations of the memory effect observed in a thin film structure with gradient U-shape like profile of Cu distribution prepared using the magnetron co-sputtering process. Structural, elemental, and band-gap analyses allowed discussion on the reason for the presence of nonpinched hysteresis in I-V plane that resulted in the observed switching effect of memory. As it was concluded based on the performed investigations, repeatable resistive switching with high difference of $6 \cdot 10^2$ times between LRS and HRS was obtained due to the formation of conducting filaments over the prepared gradient thin film. Presented results proved that thin films with gradient element distribution profile can be an interesting alternative to the conventional multilayer stack configuration for the preparation of devices utilizing memory effects.

Acknowledgment

This work was co-financed from the sources given by the Polish National Science Centre (NCN) as a research project number 2018/29/B/ST8/00548.

References

[1] S.H. Jo, T. Chang, I. Ebong, B.B. Bhadviya, P. Mazumder, W. Lu, *Nanoletters* **2010**, 10, 1297-1301;

[2] E. Gale, B. de Lacy Costello, A. Adamatzky, *Memristor Networks*, Springer, Germany **2014**.

[3] R. Lai, M. Wei, J. Wang, K. Zhou, X. Qiu, *J. Phys. D: Appl. Phys.* **2021**, 54, 015101;

[4] S. Jo Hyun, T. Chang, I. Ebong, B.B. Bhadviya, P. Mazumder, W. Lu, *Nanoletters* **2010**, 10, 1297-1301;

[5] A. Buscarino, L. Fortuna, M. Frasca, L.V. Gambuzza, *Chaos* **2012**, 22, 023136;

[6] B. Muthuswamy, L. Chua, *Int. J. Bifurc. Chaos* **2009**, 20, 1567;

[7] H. Jin-Woo, M. Meyyappan, *AIP ADVANCES* **2011**, 1, 032162;

[8] Y. Beilliard, F. Paquette, F. Brousseau, S. Ecoffey, F. Alibart, D. Drouinet, *Nanotechnology* **2020**, 31, 445205;

[9] S. Slesazeck, T. Mikolajick, Nanotechnology, **2019**, 30, 352003;

[10] F. Zahoor, T.Z. Azni Zulkifli, F.A. Khanday, *Nanoscale Res. Lett.* **2020**, 15, 90;

[11] R. Marani, G. Gelao, A.G. Perri, *Digital Library of Cornell University* **2017** (arXiv:1506.06899), https://arvix.org

[12] P. Mazumder, S.M. Kang, R. Waser, *Proc. IEEE* **2021**, 100 (6), 1911-1919;

[13] P. Parreira, S. McVitie, D.A. MacLaren, *J. Phys. Conf. Ser.* **2014**, 522, 012045;

[14] A. Chen, S. Haddad, W. Yi-Ching, T. Fang, Z. Lan, S. Avanzino, S. Pangrle, M. Buynoski, M. Rathor, W. Cai, N. Tripsas, C. Bill, M. Vanbuskirk, M. Taguchi, *Tech. Dig. − Int. Electron Devices Meet.* **2005**, 746;

[15] F. Palumbo, Ch. Wen, S. Lombardo, S. Pazos, F. Aguirre, M. Eizenberg, F. Hui, M. Lanza, *Adv. Funct. Mat.* **2020**, 30, 1900657;

[16] G. Sassine, S. La Barbera, N. Najjari, M. Minvielle, C. Dubourdieu, F. Alibrat, , *J. Vac. Sci. Technol. B* **2016**, 34, 012202;

[17] T.-T. Tan, X. Chen, T.-T. Guo, Z.-T. Liu, Chin. Phys. Lett. **2013**, 30 (10), 107302;

[18] H-Y Lee, P-S Chen, C-C Wang, S. Maikap, P-J Tzeng, C-H Lin, L-S Lee, M-J Tsai, *Japan J. Appl. Phys.* **2007**, 46, 2175-9;

[19] L-G Wang, X Qian, Z-Y Cao, G-Y Fang, A-D Li, D. Wu, *Nanoscale Res. Lett.* **2015**, 10, 135;

[20] N. Kambhala, S. Angappane, *Phys. Status Solidi B* **2017**, 254, 170020;

[21] Y. Han, K. Cho, S. Kim, *Microelectron. Eng.* **2011**, 88, 2608-2610;

[22] H. Chih-Chieh, L. Yu-Sheng, *Semicond. Sci. Technol.* **2019**, 34, 075012;

[23] B. Singh, B.R. Mehta, *TSF* **2014**, 569, 35-43;

[24] H. Chih Chieh, L. Yu-Sheng, Ch. Chao-Wen, J. Wun-Ciang, *IEEE Trans. El. Dev.* **2020**, 67 (3);

[25] J. Deuermeier, A. Kiazadeh, A. Klein, R. Martins, E. Fortunato, *Nanomaterials* **2019**, 9, 289;

[26] V. K Perla, S. K. Ghosh, K. Mallick, *Chem. Phys. Lett.* **2020**, 754, 137650;

[27] R. Dong, S.D. Lee, F.W. Xiang, J.S. Oh, J.D. Seong, H.S. Heo, J.H. Choi, J.M. Kwon, N.S. Seo, B.M. Pyun, M. Hasan, H. Hwang, *Appl. Phys. Lett.* **2007**, 90, 042107;

[28] Z. Fan, X. Fan, A. Li, L. Dong, Proc. *12th IEEE International Conference on Nanotechnology* (IEEE-NANO) **2012,** 1-4;

[29] P. Parreira, S. McVitie, D.A. MacLaren, *J. Phys.: Conf. Ser.* **2014**, 522, 012045;

[30] G. Wang, J.-H. Lee, Y. Yang, G. Ruan, D.N. Kim, Y. Ji, M.J. Tour, *Nano Lett.* **2015**, 15, 6009-6014;

[31] H.T. Park, J.S. Song, J.H. Kim, G.S. Kim, S. Chung, Y.B. Kim, J.K. Lee, M.K. Kim, J.B. Choi, S.C. Hwang, *Sci. Rep.* **2015**, 5, 15965;

[32] R. Lai, M. Wei, J. Wang, K. Zhou, X. Qiu, *J. Phys. D: Appl. Phys.* **2021**, 54, 015101;

[33] O. Heinonen, M. Siegert, A. Roelofs, A.K. Petford-Long, M. Holt, K. D'Aquila, W. Li, *Appl. Phys. Lett.* **2010**, 96, 103103;

[34] S. Seoa, M. J. Lee, D. H. Seo, E. J. Jeoung, D.-S. Suh, Y. S. Joung, I. K. Yoo, I. R. Hwang, S. H. Kim, I. S. Byun, J.-S. Kim, J. S. Choi, B. H. Parka, *Appl. Phys. Lett.* **2004**, 85, 5655;

[35] L. Goux, J.G. Lisoni, M. Jruczak, D.J. Wouters, L. Courtade, C. Muller, *J. Appl. Phys.* **2010**, 107, 024512;

[36] D.M. Pickett, B.D. Strukov, L.J. Borghetti, J.J. Yang, S.G. Snider, R.D. Stewart, R.S. Williams, *J. Appl. Phys.* **2009**, 106, 074508;

[37] W. Xiao-Ping, C. Min, Yi Shen, *Chin. Phys. B* **2015**, 24 (8), 088401;

[38] K.M. Kim, S. Han, C.S. Hwang, *Nanotechnology* **2011**, 23, 035201;

[39] N. Duraisamy, N.M. Muhammad, H-C Kim, J-D Jo, K-H Choi, *TSF* **2012**, 520, 5070-4;

[40] T.D. Dongale, S.S. Shinde, R.K. Kamat, K.Y. Rajpure, *J. Alloys Compd.* **2014**, 593, 267-70;

[41] J.J. Yang, P.J. Strachan, F. Miao, M.-X. Zhang, D.M. Pickett, W. Yi, A.A.D. Ohlberg, G. Medeiros-Riberio, S.R. Williams, *Appl. Phys. A* **2011**, 102, 785-789;

[42] Z.J. Chew, L. Li, *Mater. Lett.* **2013**, 91, 298-300;

[43] D. Chu, A. Younis, S. Li, *J. Phys. D: Appl. Phys.* **2012**, 45, 355306;

[44] J. Domaradzki, T. Kotwica, M. Mazur, D. Kaczmarek, D. Wojcieszak, *Semicond. Sci. Technol.* **2018**, 33, 015002;

[45] J. Domaradzki, *Surf. Coat. Technol.* **2016**, 290, 28-33;

[46] J. Domaradzki, D. Kaczmarek, B. Adamiak, J. Dora, S. Maguda, *PL 221077* **2011**.

[47] J. Domaradzki, M. Mazur, T. Kotwica, *Mat. Sci. Semicond. Proc.* **2018**, 87, 167-173;

[48] M. Mazur, J. Domaradzki, D. Wojcieszak, D. Kaczmarek, *Surf. Coat. Technol.* **2018**, 334, 150-157;

[49] J. Dora, patent, *PL 178285* **2000**.

[50] H. Seo, L.R. Baker, A. Hervier, J. Kim, L.J. Whitten, A.G. Somorjai, *Nano Letters* **2011**, 11 (2), 751-756;

[51] N. Zhang, J. Sun, H. Gong, *Coatings* **2019**, 9, 137;

[52] M.C. Biesinger, *Surf. Interface Anal.* **2017**, 49, 1325-1334;

[53] M.C. Biesinger, L.W.M. Lau, A.R. Gerson, R.St.C. Smart, *Appl. Surf. Sci.* **2010**, 257, 887-898;

[54] B.V. Crist, *Handbook of The Elements and Native Oxides*, XPS International Inc., USA, **1999**.

[55] M. Grodzicki, P. Mazur, A. Ciszewski, *Acta Phys. Pol. A* **2017**, 132, 351-353;

[56] R. Lewandków, M. Grodzicki, P. Mazur, A. Ciszewski, *Surf. Interface Anal.* **2021**, 53, 118-124;